Colloids and Surfaces A: Physicochemical and Engineering Aspects 702 (2024) 135081

Contents lists available at ScienceDirect

Colloids and Surfaces A: Physicochemical and Engineering Aspects

journal homepage: www.elsevier.com/locate/colsurfa

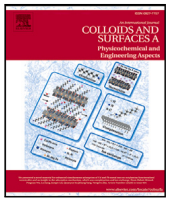

Microbubble-enhanced cold plasma activation (MB-CPA) for surface functionalization of polymer nanoparticles from nanoprecipitation

Yawen Gao [a,1], Qiuyun Lu [a,1], Shiqi Han [a], Hongyan Wu [a], Xuehua Zhang [a,b,*]

[a] Department of Chemical and Materials Engineering, University of Alberta, Alberta T6G 1H9, Canada
[b] Physics of Fluids Group, Faculty of Science and Technology, University of Twente, P.O. Box 217, 7500 AE, Enschede, Netherlands

HIGHLIGHTS

- Surface functionalization of nanoparticles in fluidic suspension by cold plasma.
- Microbubbles enhance active species transportation from air to liquid phase.
- Controlled reactive species from plasma by tuning organic solvent in liquid phase.

GRAPHICAL ABSTRACT

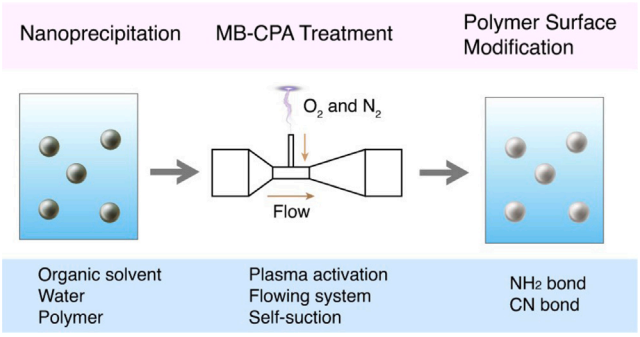

ARTICLE INFO

Keywords:
Cold plasma
Nanoprecipitation
Nanoparticles
Surface activation
Microbubbles
Flow

ABSTRACT

Cold plasma activation has been considered as a green and effective technological approach for functionalization of solid surfaces. In the current study, we introduce a versatile technique known as microbubble-enhanced cold plasma activation (MB-CPA) for surface modification of polymer plates and nanoparticles in flowing liquid phase. Corona plasma is generated at the inlet of a venturi tube, thereby creating a highly excited state in the air. Reactive nitrogen and oxygen species (RNOS) are transferred from the gas phase to the suspension flow in the form of plasma microbubbles. Two types of polymer-based nanoparticles in the suspension, namely polymethyl methacrylate (PMMA) of 16–154 nm and polycaprolactone (PCL) of 30–225 nm, are synthesized using nano-precipitation method. Through the degradation of model compounds, the polar organic solvent, acetone and ethanol, is found to promote or suppress the production of active species. In addition, the efficiency of the MB-CPA treatment depends on the solvent composition, making this technology a controllable and efficient strategy for the surface modification of nanoparticles. The findings indicate that plasma activation effectively reduces the negative surface zeta-potentials and induces aggregation and separation in the suspensions. The infrared spectra of the treated nanoparticles reveal that plasma activation leads to the formation of N–H and C–N bonds situated on the surface of PMMA. Our work demonstrates that organic-solvent involved MB-CPA emerges as a promising method for the surface modification of nanoparticles in the flow condition.

* Corresponding author at: Department of Chemical and Materials Engineering, University of Alberta, Alberta T6G 1H9, Canada.
E-mail address: xuehua.zhang@ualberta.ca (X. Zhang).
[1] Equal Contribution.

https://doi.org/10.1016/j.colsurfa.2024.135081
Received 3 July 2024; Received in revised form 31 July 2024; Accepted 12 August 2024
Available online 14 August 2024

1. Introduction

Cold plasma is characterized as a partially ionized gas, significantly enriched with reactive oxygen and nitrogen species (RNOS), offering a multitude of applications across various scientific fields [1–3]. Owing to its ability to operate without the need for hazardous chemicals, heat, or substantial mechanical energy input, cold plasma technology has emerged as a green and environmentally benign method for the synthesis and functionalization of materials [4–8]. When compared to traditional surface modification techniques, cold plasma treatment provides several distinct advantages [9]. It is particularly well-suited for processing heat-sensitive samples, which are prone to damage or decomposition under conventional treatment methods [10]. Cold plasma treatments are capable of selectively altering the chemical properties and morphology of surfaces while preserving the integrity of the bulk materials [10]. Furthermore, the degree of surface modification achievable with cold plasma can be precisely controlled through adjustments in the voltage of the electrical discharge, treatment duration and the specific configuration employed [11,12]. This precise control facilitates targeted modifications, making cold plasma an invaluable tool in the fields of materials science and engineering.

Direct exposure to cold plasma discharge in a gas phase significantly enhances the wettability and adhesion properties of solid substrates. This improvement in surface characteristics leads to better dispersion and compatibility within various liquid or solid matrices [13]. The treatment introduces functional groups onto the surface of particles, which can increase hydrophilicity, augment chemical reactivity, or facilitate strong bonding with specific molecules or substrates [14]. Furthermore, cold plasma technology offers the capability to modify the surface area, porosity, and topography of materials. It can also alter the electrical resistivity of non-planar surfaces, such as those of viscose and cotton. These modifications can result in a rougher morphology of the fiber characterized by grooves, improving the functional properties of the material [15]. Additionally, cold plasma treatment is employed to eradicate pathogens on the surfaces of fruits and vegetables, showcasing its utility in ensuring food safety and extending shelf life [16,17].

For functionalization of colloidal particles suspended in aqueous media, cold plasma activated water (PAW) serves as an effective carrier of reactive species. Air discharge and activation in a flow system provide an opportunity for the large-scale production of plasma activated water, offering significant potential for industrial applications [18]. A critical aspect of this technology is the immediate harnessing of reactive nitrogen and oxygen species (RNOS) to capitalize on their active properties for modifying colloidal particles [19]. In our recent work, cold plasma discharge was coupled with microbubbles for water treatment, called microbubble-enhanced cold plasma activation (MB-CPA) [20]. Corona plasma discharge and a venturi tube provide a source of RNOS and the flow conditions for microbubble formation. The narrow throat of the venturi tube induces a local low-pressure environment, enabling the self-suction characteristic of the tube, which promptly transfers reactive species from plasma discharge directly into the aqueous flow [21]. The microbubbles formed in the tube facilitate the mass transfer and mixing of gaseous species into the flow. This technique has demonstrated efficient degradation of various aquatic pollutants, including dyes and antibiotics, showcasing the effectiveness of MB-CPA in environmental remediation [18]. However, the application of MB-CPA for the surface functionalization of nanoparticles (NPs), particularly in a mixed-solvent system of organic solvents and water, remains unexplored. The inclusion of an organic solvent in the plasma-activated mixture could critically influence the behavior and stability of the active species, presenting a novel area for research that could lead to advancements in synthesis technology and surface engineering of NPs.

Nanoprecipitation, also named as anti-solvent precipitation, solvent shifting, and solvent displacement, is a straightforward and adaptable method for the synthesis of NPs [22–27]. NPs prepared by nanoprecipitation include polymeric NPs, inorganic NPs, active pharmaceutical ingredient NPs [28], food encapsulates with bioavailability, stability, taste and textures [29], and even oil nanodroplets or small bubbles [30–32]. In nanoprecipitation, a non-solvent is added to a solution of a solute to induce the spontaneous nucleation and growth of nanoparticles [33]. Despite its simplicity, the concentration of NPs formed via nanoprecipitation is usually low due to the intrinsic principle of nucleation and the concentration-limited growth of NPs [34,35]. Usually, NPs from nanoprecipitation need to be separated from the mixtures for further modification or surface functionalization to expand their applications or improve their functionalities [15,36]. It will simplify the process and save time if the functionalization of the surfaces of the nanoparticles can be achieved without separation from the liquid mixture for nanoprecipitation.

In this work, MB-CPA technology will be applied to modify the surface properties of NPs prepared via nanoprecipitation. For two representative polymers, polymethyl methacrylate (PMMA) and polycaprolactone (PCL), their nanoparticles with diameters less than 250 nm are formed in the mixture of water and a polar organic solvent. The influences of the presence of the polar organic solvent on the MB-CPA treatment are investigated by the degradation of model compound and surface treatment of polymer plates. We will elucidate the evolution of the size distribution, surface charges, and morphology of polymer nanoparticles with activation of the mixture flow. Our results show that MB-CPA can lead to pronounced changes in the surface properties of both types of polymer nanoparticles. Interestingly, the presence of the organic solvent in the liquid mixture can promote the activation compared to that of pure water. Our findings suggest that MB-CPA may serve as an simple and fast way to modify the surface properties of small polymer nanoparticles in a flow system.

2. Methodology

2.1. Chemicals and materials

Poly(methyl methacrylate) (PMMA: 9011-14-7, molecular weight: 120 KDa) and polycaprolactone (PCL: 24980-41-4, polycaprolactone: 80000 g/mol) were purchased from Sigma-Aldrich. PMMA plates with diameter of 34 mm and thickness of 3 mm were purchased from Enoin. The chemical structures of PMMA and PCL are shown in Fig. 1. Acetone, with a CAS number of 67-64-1 and a purity of 99.7%, was supplied by Fisher Scientific. Methyl Orange ($C_{14}H_{14}N_3O_3S{\cdot}Na$, molecular weight: 327 g/mol, purity: 98%, maximal absorption wavelength: 464 nm) and sulfathiazole ($C_9H_9N_3O_2S_2$, molecular weight: 255 g/mol, purity: 98%, maximal absorption wavelength: 284 nm) were obtained from Sigma-Aldrich and utilized as model compounds for assessing the amount of reactive oxygen species formed in MB-CPA system. Terephthalic acid (TPA, 98%) and 2-hydroxyterephthalic acid (hTPA, 97%) were purchased from Sigma-Aldrich, Canada, for the detection of hydroxyl free radicals produced during the MB-CPA treatment. Milli-Q water was obtained from a water purification system (Milli-Q, Merck, Germany) exhibiting an electrical resistivity of 18.2 MΩ · cm at a controlled temperature of 25 °C.

2.2. Preparation of polymer NPs

PMMA and PCL nanoparticles were prepared using a nanoprecipitation method [34]. Briefly, for the preparation of the polymer stock solution, PMMA was dissolved in acetone for 24 h, while it took 48 h for PCL due to its comparatively lower solubility in acetone. To enhance the solubility of both polymers, a constant temperature of 45 °C was maintained throughout the dissolution process. The nanoprecipitation procedure was meticulously followed as per established protocols. A dilute polymer solution (0.1 wt%) was prepared by dissolving 0.1 g of PMMA or PCL in 100 g of acetone. Concurrently, pure water was

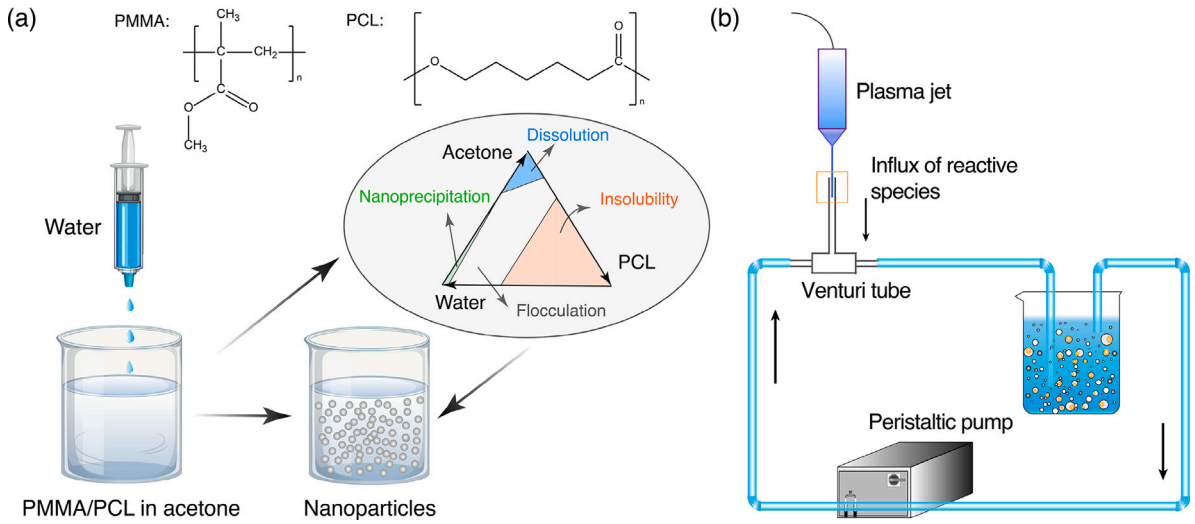

Fig. 1. Procedure of nanoprecipitation in this study (a) and the schematic of MB-CPA in the fluid for modification of nanoparticles (b) [20]. Three phase-diagram of PCL is cited from the work [37].

Table 1
Volume ratio of solution A and solution B in the preparation of polymer nanoparticles. V_A and V_W mean the volume of polymer solution and water, respectively. R_i and C_i are labeled as PMMA and PCL solutions with different volume ratios, respectively.

Sample	$R_0(C_0)$	$R_1(C_1)$	$R_2(C_2)$	$R_3(C_3)$	$R_4(C_4)$	$R_5(C_5)$	$R_6(C_6)$	$R_7(C_7)$	$R_8(C_8)$
V_A/V_W	∞	6	2	1.2	0.857	0.677	0.545	0.4615	0.4
Sample	$R_9(C_9)$	$R_{10}(C_{10})$	$R_{11}(C_{11})$	$R_{12}(C_{12})$	$R_{13}(C_{13})$	$R_{14}(C_{14})$	$R_{15}(C_{15})$	$R_{16}(C_{16})$	
V_A/V_W	0.316	0.261	0.222	0.194	0.171	0.154	0.139	0.128	

prepared as a non-solvent, as shown in Fig. 1(a). The aqueous phase, referred to as solution B, was then added dropwise to the polymer solution, designated as solution A, which comprised 6 mL of the acetone solution. This addition was performed slowly and with moderate stirring at a speed of 400 rpm to ensure optimal mixing and prevent premature precipitation. Once mixed, the stirring was promptly halted, and the resulting dispersion was immediately filtered. The volume ratios of solution A to solution B were systematically varied, as detailed in Table 1, to explore the effect of the solvent-to-nonsolvent ratios on the properties of the resulting nanoparticles.

2.3. MB-CPA treatment in a flow

The as-prepared NP solution was treated in the loop as shown in Fig. 1(b), which has been reported in our previous work [20]. MB-CPA loop system involved a plasma needle inserted into the quartz tube and a venturi tube with air inlet. Gas was drawn from the atmosphere at the air inlet of the venturi tube, where the gas was ionized by the plasma generator, and then the gaseous plasma was transferred to the liquid flow through the quartz tube, facilitated by the pressure difference [21]. This process led to the formation of plasma microbubbles containing reactive species within the venturi tube. The unique self-suction mechanism allowed the gas to enter the water without the need for a gas cylinder or a gas pump [38].

In this study, both self-made nanoparticles and the PMMA plate (diameter: 2.54 cm, thickness: 0.30 cm, Enoin) were treated using the MB-CPA loop system. To keep the treatment conditions as consistent, a PMMA plate was in-situ immersed in MB-CPA treated suspension prepared by water or the mixture of water and acetone. The mixed ratio of acetone and water was 0.128, which was the same as the nanoprecipitation method used. All dimensional parameters of MB-CPA can be referred to our previous study [18], and have been optimized to obtain a high activation efficiency. The diameter of air inlet and the length of the quartz tube connected to a venturi tube are 3 mm and 20 cm, respectively. A flow rate of 4 L/min was maintained during plasma activation in a flowing system [20].

2.4. Characteristics of polymer nanoparticles and polymer plates

The size distribution of polymer NPs prior to plasma activation was determined using dynamic light scattering (ALV/CGS-3 Goniometer). DLS measurement showed the intensity of light scattered by the particles, which correlated directly with the Brownian motion of dispersed tiny substances in the suspension medium. The intensity and pattern of the scattered light provided critical insights into the particle size distribution, allowing for the determination of their hydrodynamic radius. Notably, the size measurement capability of this DLS setup extended up to 1 μm, establishing the upper size limit for analysis based on the system's configuration and sensitivity.

The zeta potential and size distribution of polymer particles after plasma treatment were comprehensively analyzed using a Zetasizer Nano (ZEN1600, Malvern Instruments Ltd., Malvern, UK). This sophisticated instrumentation utilized a 633 nm laser beam and measures light scattering at a angle of 173°, optimal for determining the electrophoretic mobility and the zeta potential of the particles. This parameter was crucial as it reflected the surface charge and stability of colloidal systems. To ensure accuracy and reproducibility, each sample was automatically measured in triplicate automatically at 25 °C for 30 s in a small polycarbonate cell.

To characterize the surface hydrophobicity of PMMA plates, the contact angles of water on the substrates of the plates before or after the treatment of MB-CPA were measured by a contact angle meter (DSA 100, KRÜSS, Germany). To determine chemical changes in MB-CPA treatment, PMMA powders were collected by sanding both sides of PMMA plates with 100-grit sandpaper and analyzed by ATR-FTIR (Thermo Scientific Nicolet iS50, USA). The same ATR-FTIR meter was employed to characterize the functional groups present on the surface of NPs. Dry PMMA nanoparticles were collected after the evaporation of the solvent or sampled from the surface of PMMA plate after plasma activation. ATR-FTIR technique was particularly effective in identifying specific molecular bonding configurations and changes in the chemical environment of the particles.

The morphology of PMMA nanoparticles was examined by scanning electron microscope (Zeiss Sigma FESEM), operating at 5 kV with a working distance of 5.7 mm. The mixtures were drop-cast on a piece of a silicon substrate that was affixed to an aluminum SEM stub with double-sided carbon tape. Before performing SEM scanning, the deposited samples were coated with sputtered Au film with a thickness of 5 nm using vacuum film deposition equipment (Leica ACE 600). The Au film coating improves the conductivity of samples and provides better imaging during the SEM analysis.

2.5. Evaluation of MB-CPA through MO degradation in several solvent matrices

Methyl Orange solution at a concentration of 10 mg/L was prepared in a 0.5 L volume for cold plasma treatment within the MB-CPA loop. This setup employed varying solvents, including pure water, acetone/water mixture, and ethanol/water mixture. The volume ratios of acetone to water (V_A/V_W) were 0.100, 0.128, and 0.150, and the volume ratios of ethanol (V_E/V_W) to water were 0.0001, 0.005, 0.010 and 0.051. Aside from MO, sulfathiazole (STZ) was also used to estimate the efficiency of MB-CPA in ethanol and water mixture. The variance in hydroxyl free radicals formation in water or organic solvent aqueous solution was investigated by the chemical probe method coupled with fluorescence spectroscopy. TPA was used as a chemical probe and reacted with hydroxyl free radicals to form hTPA, which showed a peak fluorescence emission at 423 nm when excited by light at 310 nm. The enhanced degradation efficiency, indicative of accelerated oxidation of the dye compound, was associated with heightened formation of reactive oxygen species within the activation system. In this work, the degradation efficiency of MO was assessed via absorbance measurement using a UV-vis spectrometer (Thermo Scientific, GENESYS 150). The level of reactive oxygen species generated in MB-CPA system is indirectly reflected by the degradation efficiency of MO, referring to Beer–Lambert Law (Eq. (1)) and Eq. (2).

$$A = \varepsilon \times b \times \mathrm{C} \tag{1}$$

$$\text{Degradation efficiency (\%)} = (\mathrm{C}_0 - \mathrm{C}_t)/\mathrm{C}_0 \times 100 \tag{2}$$

where ε is molar absorptivity. b is the length of the light path in the measurement of UV-vis. C_t and C_0 denote the concentration of the solute at treatment time t and 0, respectively. A is the absorbance of the peak at 464 nm.

3. Results and discussion

3.1. Influence of acetone concentration on the reactive oxide species

The degradation of a model compound MO in water and in acetone aqueous solution was followed by the characteristic peak at 464 nm in UV–Vis spectra as shown in Fig. 2(a–d). A sharp decrease in the MO concentration occurred in the water acetone mixture after 1.5 min of treatment, while the drop of absorbance in the water was much less. As the volume ratio of acetone to water increases from 0.100 to 0.150, the degradation efficiency of MO reached 93.7% to 97.1% (Fig. 2(e)). There was no significant difference resulted from the three volume ratios of acetone in our experiments. For the same duration of 1.5 min treatment, the degradation efficiency was substantially lower in water, reaching only 54.9%. After 3 min, the solution of MO in the acetone solution was colorless from full removal of MO, while the solution in water was still light yellow, indicating insufficient degradation of MO. The energy yield of the MB-CPA-driven MO degradation was measured, which decayed with the treatment time. The difference among acetone solution with different volume ratio was negligible. In the first 3 min, the energy yield in the acetone solution was over 1.7 times larger than that in water. The highest energy yield was achieved in the acetone aqueous solution with V_A/V_W of 0.150.

The significant enhancement of the MO degradation efficiency in the acetone water mixtures could be attributed to two possible reasons. Acetone was more volatile than water. With a lower vapor pressure, an acetone aqueous solution formed more vapor bubbles than water under the same pressure reduction in the venturi tube as shown in Fig. 2(g). In addition, the surface tension of an acetone aqueous solution was lower than that in water, which also promoted the formation of microbubbles [18]. A larger amount of microbubbles improved the transfer efficiency of ROS generated from the plasma discharge in air, a key feature of the MB-CPA process. The higher concentration of hydroxyl free radicals (·OH), as a dominant ROS contributing to the degradation of MO, in the acetone aqueous solution also validated the effect of more microbubbles (Fig. 2(g)). As the volume ratio of acetone to water increased from 0.100 to 0.150, the interfacial tension of the acetone water mixture only changed from 53 to 48 N/m [39]. Therefore, the influence on interfacial tension from acetone concentration was negligible, resulting in similar degradation rates of MO. Another reason could be that the degradation pathway of MO may differ due to the presence of acetone, which needs further exploration. The low-concentration acetone aqueous solution was treated by the same setup and the absorbance curves of the acetone solution remain identical after the treatment (Fig. 2(h)). Therefore, the possibility of acetone as another source of ROS was excluded.

As an alternative organic solvent, ethanol was also added into the liquid phase for the degradation of model compounds in MB-CPA treatment. The degradation efficiency of MO and STZ was also dependent on the ratio of ethanol in the liquid phase. When the ethanol-to-water volume ratio (V_E/V_W) was 0.010, the degradation efficiency of MO is similar to that in water but less than that in the mixture with V_E/V_W of 0.053 (Fig. 3(a)). As the flow rate varied among 3, 4, and 5 L/min, the degradation efficiency of MO in the ethanol aqueous solution with V_E/V_W of 0.053 kept higher than that in the control group (Fig. 3(b)). Furthermore, the degradation of MO was faster as the liquid flow rate increases, but such influence was less significant on the treatment in the ethanol/water mixture than that in water. For the degradation of STZ, the solution with V_E/V_W of 0.010 provided the highest degradation efficiency compared with the ratio of 0.005 and 0.0001 (Fig. 3(c)). STZ degraded with a similar rate in the solution with V_E/V_W of 0.005 and pure water but degrades much slower as the ratio further decreased to 0.0001. Generally, the results suggested that the organic solvent, such as ethanol, could either promote or suppress the formation of reactive oxygen species during the MB-CPA treatment by adjusting the solvent type and ratio.

3.2. Influence of treatment methods on PMMA plate

Fig. 4 showed the changes in the surface wetting property and functional groups of a PMMA plate exposed to plasma activated water and an acetone aqueous solution. The surface of the PMMA plate increased slightly by 10 and 5 degrees after the MB-CPA treatment in water and acetone water mixture, respectively. In the FTIR spectra (Fig. 4(f)), there were a group of characteristic peaks in the region 700 to 1750 cm^{-1} assigned to PMMA at the wave number of 988, 1144, 1237, 1396, 1457, 1725 cm^{-1}. After MB-CPA treatment, compared to the untreated group, the peak at 1536 cm^{-1} became higher after exposed to plasma activation. The peak intensity was even stronger in the group using an acetone aqueous solution as the liquid matrix. A new peak at 1323 cm^{-1} appeared in the MB-CPA treated PMMA and was stronger in the acetone aqueous solution than in water.

The peak at 1536 cm^{-1} may be assigned to the –N-H- bending in amino groups. The enhancement in the signals from amine groups may be attributed to the surface reaction of PMMA with plasma-generated nitrogen species [40]. Formation of the peak at 1323 cm^{-1} could be attributed to the newly forming -CHO group on the PMMA surface during the MB-CPA treatment. The results clearly demonstrated that the active species from MB-CPA could effectively modify the PMMA surface.

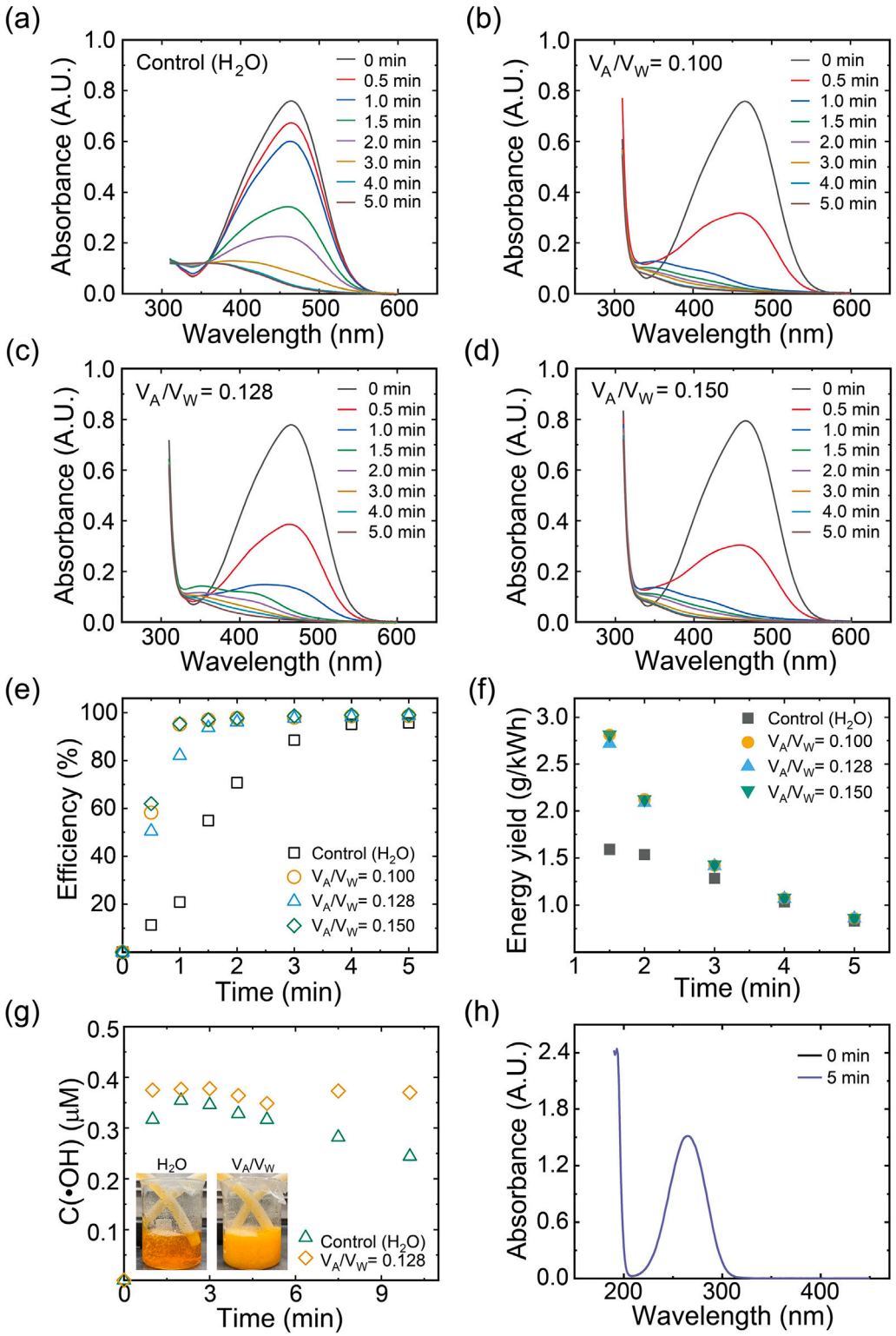

Fig. 2. UV–Vis spectra of MO solutions with treatment time in water (a) and in the solution with the volume ratio of acetone at 0.100 (b), 0.128 (c), 0.150 (d). (e) Degradation efficiency and (f) energy yield of MO degradation with the treatment time. (g) Concentrations of hydroxyl free radicals in water or acetone aqueous solution (V_A/V_W = 0.128). Photos of the bubble generated in two liquid matrices were attached (at 20 s of MB-CPA treatment) (h) Absorbance spectra of acetone water mixture (V_A/V_W = 0.006) before and after the MB-CPA treatment of 5 min. Two lines were overlapped with each other.

3.3. Size distribution of polymeric nanoparticles

MB-CPA treatment showed the potential of altering the surface hydrophobicity and functional groups of polymer plates in a flowing aqueous phase. The effect of this technology on the nano-sized polymeric colloids was further explored by using PMMA and PCL nanoparticles as examples. PMMA and PCL nanoparticles were produced using 16 different compositions of polymer solutions with several proportions of water. The volume ratios of acetone to water ranged from 6 to 0.128 (Table 1). After adding the desired volume of water, the

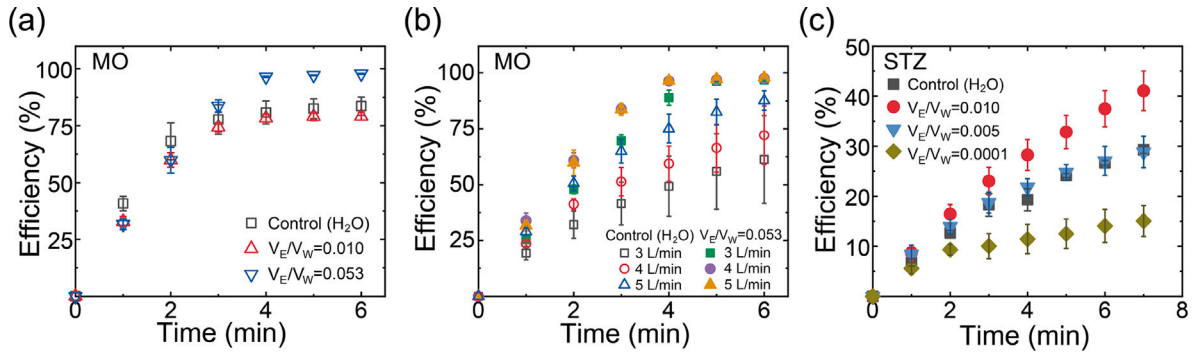

Fig. 3. (a) Degradation efficiency of MO with the MB-CPA treatment duration (0-6 min) in water (control) or ethanol/water solution with V_E/V_W of 0.010 and 0.053, with the liquid flow rate of 4 L/min. (b) Degradation efficiency of MO in MB-CPA treatment with liquid flow rate of 3, 4, and 5 L/min in either water or ethanol aqueous solution (V_E/V_W of 0.053). (c) Degradation efficiency of STZ with the MB-CPA treatment duration (0–7 min) in water or ethanol/water solution with V_E/V_W of 0.0001. 0.005, and 0.010, with the liquid flow rate of 4 L/min.

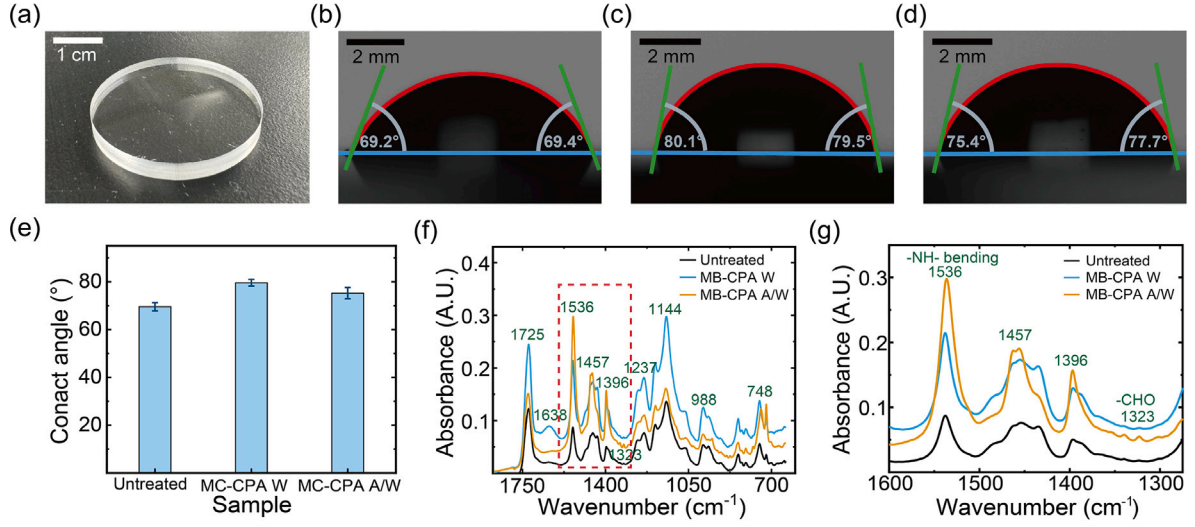

Fig. 4. (a) Untreated PMMA plate applied in this study (scale bar: 1 cm). Contact angles of water on PMMA plates (b) without plasma treatment and with plasma treatment (c) in water and (d) the mixture of water and acetone (V_A/V_W=0.128). (e) Average contact angles of water droplets for the series of groups above. (f) ATR-FTIR spectra of powders collected from pristine PMMA plate, PMMA plates treated in water or acetone water mixture (V_A/V_W=0.128). (g) Zoomed-in ATR-FTIR spectrum of (f) (1275 to 1600 cm^{-1}).

images of the mixture were shown in Fig. 5(a). At the start of mixing, a faintly opalescent suspension was obtained (R_0-R_8). With more volume of water added to a higher diluted level (R_9-R_{16}), the mixtures were more opaque.

As shown in Fig. 5(b), the size distribution of PMMA nanoparticles varied with composition of the mixtures. With more water added, the range of size distribution of PMMA nanoparticles became more narrow with smaller size. For example, The size distribution of R_3 was located from 22.13 nm to 180 nm. As the ratio decreased to R_{16}, the size range of polymer nanoparticles was from 33 nm to 50 nm.

Fig. 6 showed the preparation and size distribution of PCL suspensions. PCL particles formed by the nanoprecipitation method were comparatively larger than PMMA particles due to their intrinsic properties. A few suspensions consisted of large particles had exceeded the limitation of DLS detection (1 μm). In Fig. 6(a), with the volume of water increased (from C_3 to C_{16}), small and uniformed nanoparticles were formed, ranging from 865 nm (C_3) to 40.5 nm (C_{15}). As the composition reached C_{16}, the size of the PCL particles with the highest intensity decreased to 149.5 nm. The uniform nanoparticle suspensions were selected for the following experiments by MB-CPA treatment: R_{16} and C_{16} for PMMA and PCL nanoparticle suspensions, respectively.

During the nanoprecipitation process, various factors affect the suspensions of stable nanoparticles with the desired size and properties, for example, the components of the polymer, the speed of mixing and stirring, the ratio between the organic solution and non-solvent, and the temperature [24]. Most importantly, to obtain a smaller size of nanoparticles in suspension, the initial polymer concentration should be low so that it provides sufficient nucleation sites for the growth of nanoparticles. Miladi et al. reported that polymer molecular weight affected particle size in the nanoprecipitation process. The smaller particles size with high molecular wight could be explained by faster precipitation [41,42]. In contrast, the induced large particle size was explained by the higher viscosity of the liquid system [43]. However, the further specific explanation was not well explored on this aspect. Lebouille et al. reported that the fast mixing time and polymer concentration were important, while the molar mass of polymer had little effect for the size evolution in PCL-acetone system [44].

3.4. Effects of MB-CPA on size distribution and surface properties

Plasma activation was employed to activate nanoparticles using the setup of microbubble-enhanced cold plasma activation. The zeta potentials of nanoparticles were measured as shown in Fig. 7(a). The initial values for PMMA and PCL without plasma activation were −33.17 mV and −23.13 mV, respectively, consistent with the value in the literature [45].

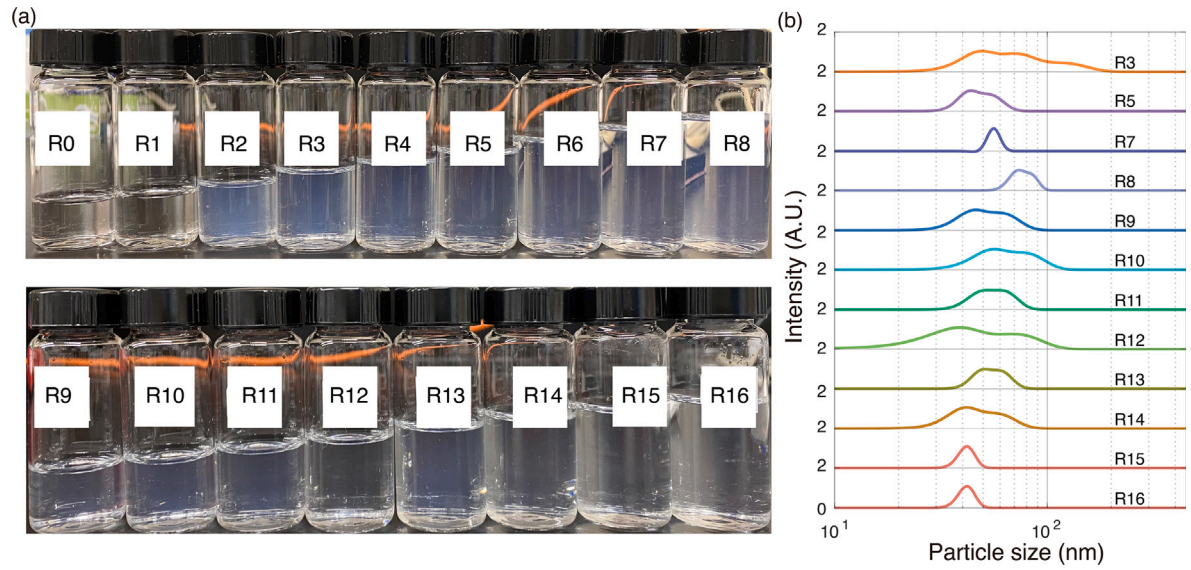

Fig. 5. (a) Nanoprecipitation of PMMA polymer solution with various ratios of acetone solution and water. (b) Several solutions were selected to measure the size distribution by DLS. The legends in the plots correspond to the labels on the sample bottles.

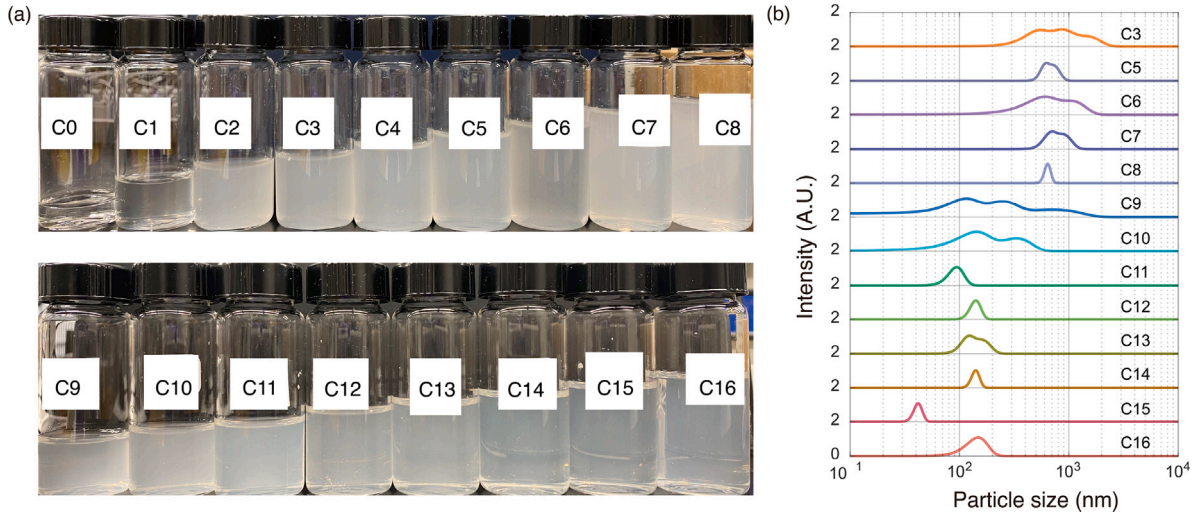

Fig. 6. (a) Nanoprecipitation of PCL polymer solution with various ratios of acetone solution and water. (b) Several solutions were selected to measure the size distribution by DLS. The legends in the plots correspond to the labels on the sample bottles.

From the initial 20 min of treatment, the potential was almost constant for PMMA nanoparticles, and decreased slightly for PCL nanoparticles. In further treatment, the zeta potentials of both nanoparticles increased with activation time. After 60 min activation, the zeta potentials increased to −10 mV for both PMMA and PCL nanoparticles.

The surface charge of the particles became more positive, implying a lower repulsion force between the particles. Zeta potential represented the quantification of electrophoretic mobility of materials in solution, depending on the polarity (charge) of the adsorbed counter ions in the electric double layer, and the ionic concentration of the solvent [46]. According to the results in Fig. 7(a), the zeta potential of PMMA almost increased throughout the treatment with MB-CPA, which may be attributed to the formation of amine groups.

The rate of the potential increase was almost same for PCL and PMMA nanoparticles, although these two polymers had different reactivity. Both polymers can undergo oxidation, but the extent and rate of oxidation varied depending on treatment conditions, chemical structure and the additives or impurities involved. The same rate in the potential increase suggested that the reactions between the active species and the polymer surface might be limited by the factor, such as the concentration of active species generated from MB-CPA. Our earlier work showed that the degradation of micropollutants in water by MB-CPA was also limited by the active species [18].

During plasma treatment of polymer nanoparticles in suspension, significant changes in particle size were observed, as depicted in Fig. 7(b). Specifically, the application of plasma led to an increase in the mean size of PMMA particles from 144 nm at time zero to 927 nm at time 60 min, primarily due to the formation of aggregates within the suspension. This aggregation phenomenon was attributed to plasma-induced cross-linking and molecular interactions among PMMA molecules. In contrast, the behavior of PCL nanoparticles under similar conditions exhibited a different pattern. Mean diameter of PCL detected decreased from 479 nm at time zero to 136 nm at 20 min, then it almost kept a stable value within the next 30 min. At the onset of plasma treatment, larger PCL particles tended to aggregate more readily, resulting in the formation of a polymer film that floated to the surface of the suspension. Consequently, the size of the remaining PCL particles in the lower part of the suspension which were collected for

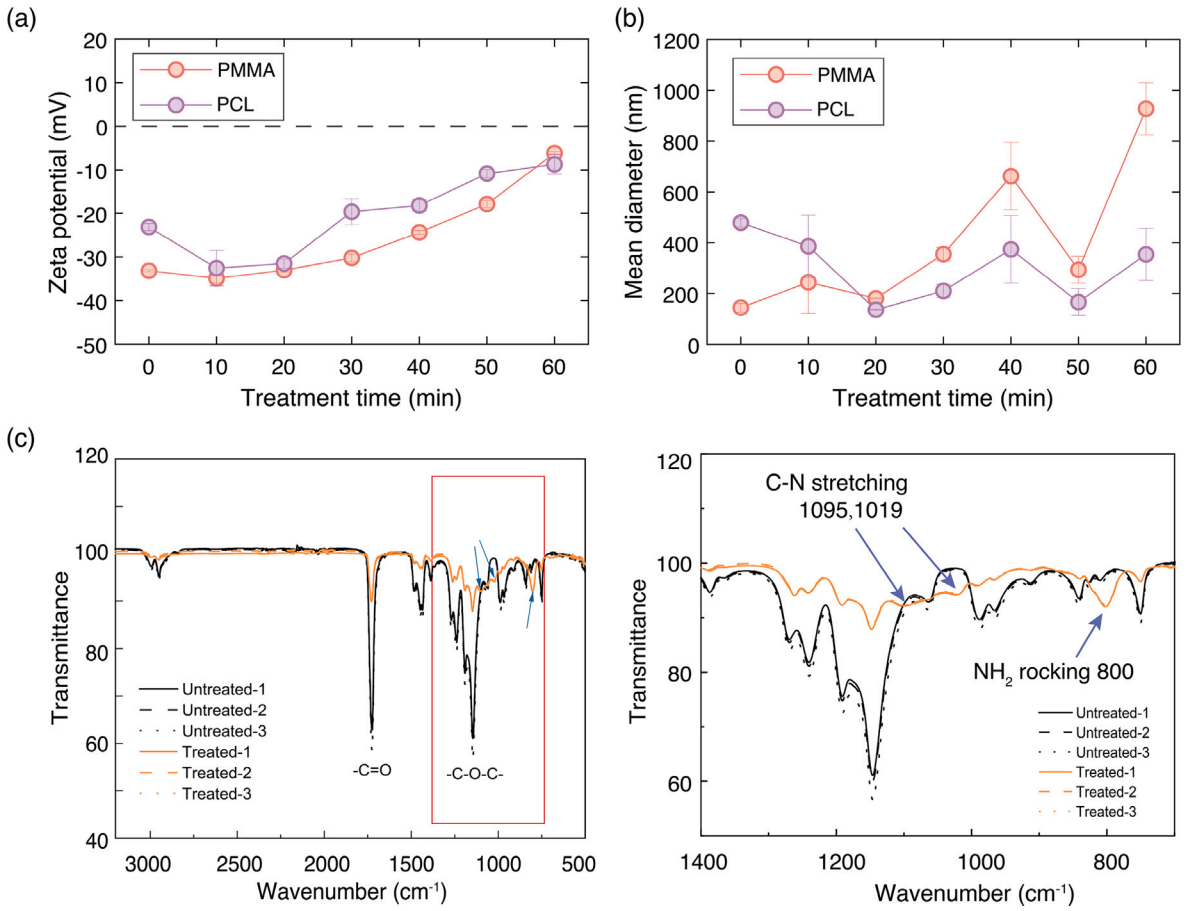

Fig. 7. (a) Values of zeta-potential of PMMA and PCL suspensions as a function of activation time with connected lines. (b) The mean diameter of PMMA and PCL polymer particles measured by zeta-sizer during cold plasma activation. (c) Infrared spectra of pristine PMMA particles (black lines) and treated ones (orange lines) with cold plasma activation. Right Figure is the part of spectra of the left after zooming in. The arrows point to the typically changed peaks of FTIR spectra.

the detection initially decreased, reflecting the removal of larger particles through aggregation. Following this initial decrease, the size of the PCL particles stabilized, maintaining a consistent value, as illustrated by the comparably stable line. This stabilization suggested a dynamic equilibrium between the aggregation and dispersion processes in the plasma-treated PCL suspension, highlighting the distinct responses of different polymer materials to plasma exposure.

Fig. 7(c) showed the ATR-FTIR spectra of PMMA particles. Compared to pristine PMMA particles, three new peaks appeared, indicating C–N stretching at 1019 nm and 1095 nm and NH_2 at 800 nm, respectively. Cold plasma could impact the chemical properties of solid particles, showing the surface modification by chemical bonds [47]. Reactive nitrogen species generated by nitrogen discharge interacted with the surface of the polymer. Therefore, plasma activation can achieve surface functionalization by adding nitrogen chemical bonds.

Similar phenomena have also been observed in other works. Bormashenko et al. reported that the -CH_2 groups generated from plasma activation from the surface of the polymer trap the ions, accompanied by surface charging [48]. The formation of active sites was due to the excited species produced with free electrons with cold plasma. The interaction of these excited species led to the chemical functionalization on the surface, incorporating –OH, –CO, and –COOH [49]. Moreover, reactive species triggered by cold plasma caused further chemical reactions, showing as cross-linking, etching and chemical modification [50]. Bruser et al. stated that the nitrogen plasma was capable of increasing functional groups such as –C–OH, C–O–C–, O=C–O, pyridine, and quaternary nitrogen groups [51]. Therefore, plasma treatment is a potential alternative that can be used for the surface functionalization of small particles.

The morphology and size distribution of PMMA nanoparticles before and after cold plasma treatment were investigated by SEM, as shown in Fig. 8. Spherical-shaped PMMA nanoparticles produced by nanoprecipitation (recipe R_{16}) were observed in the nano-scale. After treating the PMMA nanoparticle suspension with the MB-CPA reactor, adhesion of particles with aggregates formed among the nanoparticles, as shown in Fig. 8(b). The increase in the surface charge of PMMA also reflected the possibility of forming aggregates. The size distribution of PMMA nanoparticles before and after MB-CPA treatment was demonstrated in Fig. 8(e) and (f) after the segmentation by Image J and Cellpose [52]. The peak frequency of pristine PMMA nanoparticles appeared at a radius of 43 nm. The size peak of MB-CPA-treated PMMA nanoparticles was located at around 26 nm, 40% less than that of pristine PMMA particles. The ratio of particles with the size between 3 to 20 nm also obviously increased.

Due to the segmentation step, the size distribution in Fig. 8 neglected the adhesion and bridging area between particles, especially in the condition after the MB-CPA treatment. However, the connected nanoparticles may be recognized as one part in the measurement by Zeta sizer. This explained why larger diameter is resented in Fig. 7(b), while smaller size was revealed in SEM images.

In this work, the influences of acetone on the production of reactive species and surface modification of polymeric nanoparticles are mainly discussed. However, surface modification is not limited to acetone-water-polymer ternary systems, but may be expanded to other ternary systems, for example, with ethanol as an organic (co-)solvent. By controlling the type and ratio of organic solvent, the reactive species generated during MB-CPA may correspondingly change, realizing versatile applications.

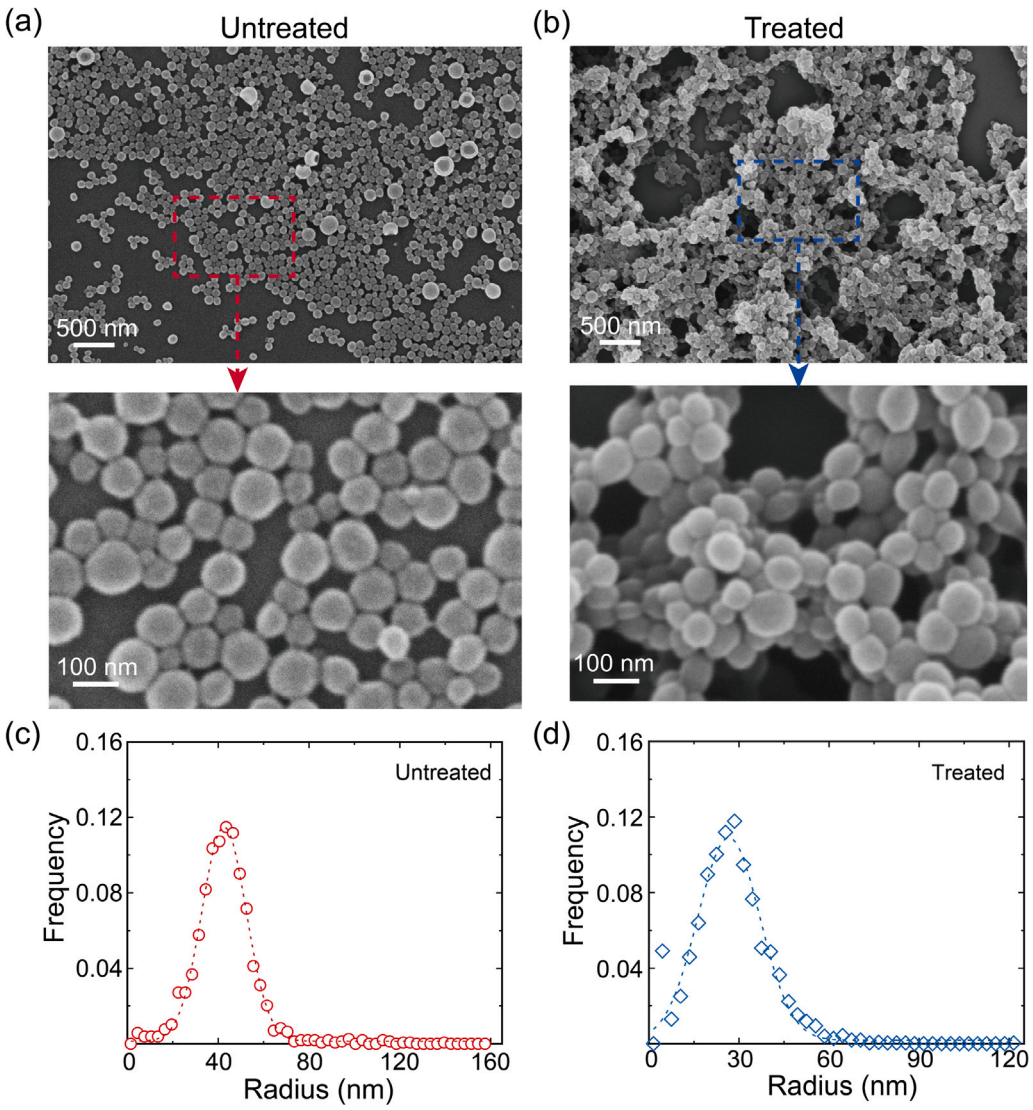

Fig. 8. SEM images of PMMA nanoparticles prepared by nanoprecipitation method without cold plasma treatment (a) and with cold plasma treatment for 30 min (b). The zoomed-in images are in the second row. The corresponding size distribution of PMMA nanoparticles without (c) and with (d) cold plasma treatment.

4. Conclusions

In this work, the effect of microbubble-enhanced cold plasma activation (MB-CPA) on the surface of polymer nanoparticles has been investigated in a flowing system. As demonstrated in the higher degradation rate of a model compound and stronger absorbance from the newly formed functional groups on the surface of PMMA plates, we show that the presence of acetone or ethanol in the flowing liquid loop alters the production efficiency of reactive species during MB-CPA. Both PMMA and PCL nanoparticles, prepared by nanoprecipitation method, show a reduction in the negative charge upon the cold plasma treatment, accompanied with the formation of aggregation in the suspension, as confirmed through size analyzer and SEM imaging. MB-CPA treatment facilitates the formation of nitrogen-containing functional groups such as C–N and N–H groups on the surface of nanoparticles, showcasing the potential of cold plasma techniques in enabling chemical modifications without the need for additional chemical agents. These findings suggest that MB-CPA can be a powerful tool for the tailored functionalization of nanoparticle surfaces, essential for enhancing their compatibility and functionality in diverse applications. Future work will focus on refining the control over the functionalization process and expanding the applicability of this technology to other types of materials and industrial processes. This could potentially lead to the development of a new class of highly functional, plasma-treated nanomaterials, tailored for specific applications in a sustainable and economically feasible manner.

CRediT authorship contribution statement

Yawen Gao: Writing – review & editing, Writing – original draft, Visualization, Validation, Methodology, Investigation. **Qiuyun Lu:** Writing – review & editing, Writing – original draft, Visualization, Validation, Methodology, Investigation. **Shiqi Han:** Visualization. **Hongyan Wu:** Visualization, Validation, Methodology. **Xuehua Zhang:** Writing – review & editing, Validation, Supervision, Funding acquisition, Conceptualization.

Declaration of competing interest

The authors declare that they have no known competing financial interests or personal relationships that could have appeared to influence the work reported in this paper.

Data availability

Data will be made available on request.

Acknowledgments

This project is supported by China Scholarship Council (201906370041), the Natural Science and Engineering Research Council of Canada (NSERC)-Mitacs collaborative program, Alberta Innovates, Canada Research Chair Program (Award number: CRC-2018-00344), and NSERC Discovery Project. We thank the help from Dr. Qing Sun from the Hunan Normal University (China) for the measurements of zeta-potential.

References

[1] R. Zhou, R. Zhou, P. Wang, Y. Xian, A. Mai-Prochnow, X. Lu, P. Cullen, K.K. Ostrikov, K. Bazaka, Plasma-activated water: Generation, origin of reactive species and biological applications, J. Phys. D: Appl. Phys. 53 (30) (2020) 303001.

[2] Y. Gao, K. Francis, X. Zhang, Review on formation of cold plasma activated water (PAW) and the applications in food and agriculture, Food Res. Int. 157 (2022) 111246.

[3] N. Kaushik, S. Mitra, E.J. Baek, L.N. Nguyen, P. Bhartiya, J.H. Kim, E.H. Choi, N.K. Kaushik, The inactivation and destruction of viruses by reactive oxygen species generated through physical and cold atmospheric plasma techniques: Current status and perspectives, J. Adv. Res. 43 (2023) 59–71.

[4] H. Jiang, F. Chen, M.G. Lagally, F.S. Denes, New strategy for synthesis and functionalization of carbon nanoparticles, Langmuir 26 (3) (2010) 1991–1995.

[5] B. Ouyang, Y. Zhang, Y. Wang, Z. Zhang, H.J. Fan, R.S. Rawat, Plasma surface functionalization induces nanostructuring and nitrogen-doping in carbon cloth with enhanced energy storage performance, J. Mater. Chem. A 4 (45) (2016) 17801–17808.

[6] A. Dey, A. Chroneos, N.S.J. Braithwaite, R.P. Gandhiraman, S. Krishnamurthy, Plasma engineering of graphene, Appl. Phys. Rev. 3 (2) (2016).

[7] S.K. Pankaj, K.M. Keener, Cold plasma: Background, applications and current trends, Curr. Opin. Food Sci. 16 (2017) 49–52.

[8] V. Sethi, C. Verma, S. Mukhopadhyay, A. Gupta, B. Gupta, Oxidative functionalization of polypropylene mesh surface by radio frequency plasma, Surf. Interfaces 37 (2023) 102656.

[9] H. Zhang, P. Li, A. Zhang, Z. Sun, J. Liu, P. Héroux, Y. Liu, Enhancing interface reactions by introducing microbubbles into a plasma treatment process for efficient decomposition of PFOA, Environ. Sci. Technol. 55 (23) (2021) 16067–16077.

[10] S.K. Nemani, R.K. Annavarapu, B. Mohammadian, A. Raiyan, J. Heil, M.A. Haque, A. Abdelaal, H. Sojoudi, Surface modification of polymers: methods and applications, Adv. Mater. Interfaces 5 (24) (2018) 1801247.

[11] S. Kumar, R. Singh, T.P. Singh, B.L. Sethi, Surface modification by electrical discharge machining: A review, J. Mater. Process. Technol. 209 (8) (2009) 3675–3687.

[12] Y. Liu, X. Shen, J. Sun, P. Li, A. Zhang, Treatment of aniline contaminated water by a self-designed dielectric barrier discharge reactor coupling with microbubbles: optimization of the system and effects of water matrix, J. Chem. Technol. Biotechnol. 94 (2) (2018) 494–504.

[13] L. Carrino, G. Moroni, W. Polini, Cold plasma treatment of polypropylene surface: a study on wettability and adhesion, J. Mater. Process. Technol. 121 (2–3) (2002) 373–382.

[14] Y. Liu, J. He, Y. Sun, J. Hu, C. Li, G. Xue, S. Ognier, A comparison of N-doped TiO_2 photocatalysts preparation methods and studies on their catalytic activity, J. Chem. Technol. Biotechnol. 88 (10) (2013) 1815–1821.

[15] M.J. Macedo, G.S. Silva, M.C. Feitor, T.H. Costa, E.N. Ito, J.D. Melo, Surface modification of kapok fibers by cold plasma surface treatment, J. Mater. Res. Technol. 9 (2) (2020) 2467–2476.

[16] C. Liu, C. Chen, A. Jiang, X. Sun, Q. Guan, W. Hu, Effects of plasma-activated water on microbial growth and storage quality of fresh-cut apple, Innov. Food Sci. Emerg. Technol. 59 (2020) 102256.

[17] Q. Xiang, L. Fan, Y. Li, S. Dong, K. Li, Y. Bai, A review on recent advances in plasma-activated water for food safety: Current applications and future trends, Crit. Rev. Food Sci. Nutr. 62 (8) (2022) 2250–2268.

[18] Y. Gao, M. Li, C. Sun, X. Zhang, Microbubble-enhanced water activation by cold plasma, Chem. Eng. J. 446 (2022) 137318.

[19] J. Zhao, A. Zhang, P. Heroux, Z. Sun, Y. Liu, Remediation of diesel fuel polluted soil using dielectric barrier discharge plasma, Chem. Eng. J. 417 (2021) 128143.

[20] Y. Gao, Z. Saedi, H. Shi, B. Zeng, B. Zhang, X. Zhang, Machine learning-assisted optimization of microbubble-enhanced cold plasma activation for water treatment, ACS ES&T Water (2024).

[21] Y. Gao, A.M. Dashliborun, J.Z. Zhou, X. Zhang, Formation and stability of cavitation microbubbles in process water from the oilsands industry, Ind. Eng. Chem. Res. 60 (7) (2021) 3198–3209.

[22] H. Fessi, F. Puisieux, J.P. Devissaguet, N. Ammoury, S. Benita, Nanocapsule formation by interfacial polymer deposition following solvent displacement, Int. J. Pharm. 55 (1) (1989) R1–R4.

[23] Y. Liu, G. Yang, D. Zou, Y. Hui, K. Nigam, A.P. Middelberg, C.-X. Zhao, Formulation of nanoparticles using mixing-induced nanoprecipitation for drug delivery, Ind. Eng. Chem. Res. 59 (9) (2019) 4134–4149.

[24] S. Göttert, I. Salomatov, S. Eder, B.C. Seyfang, D.C. Sotelo, J.F. Osma, C.K. Weiss, Continuous nanoprecipitation of polycaprolactone in additively manufactured micromixers, Polymers 14 (8) (2022) 1509.

[25] J. Tao, S.F. Chow, Y. Zheng, Application of flash nanoprecipitation to fabricate poorly water-soluble drug nanoparticles, Acta Pharmaceutica Sinica B 9 (1) (2019) 4–18.

[26] H.A. Almoustafa, M.A. Alshawsh, Z. Chik, Technical aspects of preparing PEG-PLGA nanoparticles as carrier for chemotherapeutic agents by nanoprecipitation method, Int. J. Pharm. 533 (1) (2017) 275–284.

[27] S. Hornig, T. Heinze, C.R. Becer, U.S. Schubert, Synthetic polymeric nanoparticles by nanoprecipitation, J. Mater. Chem. 19 (23) (2009) 3838–3840.

[28] S. Khan, M. Naushad, A. Al-Gheethi, J. Iqbal, Engineered nanoparticles for removal of pollutants from wastewater: Current status and future prospects of nanotechnology for remediation strategies, J. Environ. Chem. Eng. 9 (5) (2021) 106160.

[29] C.J.M. Rivas, M. Tarhini, W. Badri, K. Miladi, H. Greige-Gerges, Q.A. Nazari, S.A.G. Rodríguez, R.Á. Román, H. Fessi, A. Elaissari, Nanoprecipitation process: From encapsulation to drug delivery, Int. J. Pharmaceutics 532 (1) (2017) 66–81.

[30] Z. Lu, M.H.K. Schaarsberg, X. Zhu, L.Y. Yeo, D. Lohse, X. Zhang, Universal nanodroplet branches from confining the Ouzo effect, Proc. Natl. Acad. Sci. 114 (39) (2017) 10332–10337.

[31] D. Lohse, X. Zhang, et al., Surface nanobubbles and nanodroplets, Rev. Modern Phys. 87 (3) (2015) 981.

[32] X. Zhang, D. Lohse, Perspectives on surface nanobubbles, Biomicrofluidics 8 (4) (2014).

[33] A. Minost, J. Delaveau, M.-A. Bolzinger, H. Fessi, A. Elaissari, Nanoparticles via nanoprecipitation process, Recent Patents Drug Deliv. Formulation 6 (3) (2012) 250–258.

[34] J. Aubry, F. Ganachaud, J.-P. Cohen Addad, B. Cabane, Nanoprecipitation of polymethylmethacrylate by solvent shifting: 1. Boundaries, Langmuir 25 (4) (2009) 1970–1979.

[35] F. Bally, D.K. Garg, C.A. Serra, Y. Hoarau, N. Anton, C. Brochon, D. Parida, T. Vandamme, G. Hadziioannou, Improved size-tunable preparation of polymeric nanoparticles by microfluidic nanoprecipitation, Polymer 53 (22) (2012) 5045–5051.

[36] F. Gao, An overview of surface-functionalized magnetic nanoparticles: preparation and application for wastewater treatment, ChemistrySelect 4 (22) (2019) 6805–6811.

[37] S. Schubert, J.T. Delaney Jr., U.S. Schubert, Nanoprecipitation and nanoformulation of polymers: from history to powerful possibilities beyond poly (lactic acid), Soft Matter 7 (5) (2011) 1581–1588.

[38] Z. Saedi, M. Kuddushi, Y. Gao, D. Panchal, B. Zeng, S.E. Pour, H. Shi, X. Zhang, Stable and efficient microbubble-enhanced cold plasma activation for treatment of flowing water, Sustain. Mater. Technol. 40 (2024) e00887.

[39] K.S. Howard, R. McAllister, Surface tension of acetone-water solutions up to their normal boiling points, AIChE J. 3 (3) (1957) 325–329.

[40] G. Duan, C. Zhang, A. Li, X. Yang, L. Lu, X. Wang, Preparation and characterization of mesoporous zirconia made by using a poly (methyl methacrylate) template, Nanoscale Res. Lett. 3 (2008) 118–122.

[41] F. Lince, D.L. Marchisio, A.A. Barresi, Strategies to control the particle size distribution of poly-ε-caprolactone nanoparticles for pharmaceutical applications, J. Colloid Interface Sci. 322 (2) (2008) 505–515.

[42] K.P. Seremeta, D.A. Chiappetta, A. Sosnik, Poly (ε-caprolactone), Eudragit® RS 100 and poly (ε-caprolactone)/Eudragit® RS 100 blend submicron particles for the sustained release of the antiretroviral efavirenz, Colloids Surf. B 102 (2013) 441–449.

[43] I.L. Blouza, C. Charcosset, S. Sfar, H. Fessi, Preparation and characterization of spironolactone-loaded nanocapsules for paediatric use, Int. J. Pharm. 325 (1–2) (2006) 124–131.

[44] J. Lebouille, R. Stepanyan, J. Slot, M.C. Stuart, R. Tuinier, Nanoprecipitation of polymers in a bad solvent, Colloids Surf. A 460 (2014) 225–235.

[45] I.Y. Perevyazko, A. Vollrath, C. Pietsch, S. Schubert, G.M. Pavlov, U.S. Schubert, Nanoprecipitation of poly (methyl methacrylate)-based nanoparticles: Effect of the molar mass and polymer behavior, J. Polym. Sci. A: Polym. Chem. 50 (14) (2012) 2906–2913.

[46] M. Hage, S. Khelissa, H. Akoum, N.-E. Chihib, C. Jama, Cold plasma surface treatments to prevent biofilm formation in food industries and medical sectors, Appl. Microbiol. Biotechnol. (2022) 1–20.

[47] A. Yusuf, H.K. Amusa, J.O. Eniola, A. Giwa, O. Pikuda, A. Dindi, M.R. Bilad, Hazardous and emerging contaminants removal from water by plasma-based treatment: A review of recent advances, Chem. Eng. J. Adv. (2023) 100443.

[48] E. Bormashenko, G. Whyman, V. Multanen, E. Shulzinger, G. Chaniel, Physical mechanisms of interaction of cold plasma with polymer surfaces, J. Colloid Interface Sci. 448 (2015) 175–179.

[49] O.S. Kolluri, Application of Plasma Technology for Improved Adhesion of Materials, CRC Press, 2003.
[50] Y. Wen, C. Shen, Y. Ni, S. Tong, F. Yu, Glow discharge plasma in water: a green approach to enhancing ability of chitosan for dye removal, J. Hazard. Mater. 201 (2012) 162–169.
[51] V. Brüser, M. Heintze, W. Brandl, G. Marginean, H. Bubert, Surface modification of carbon nanofibres in low temperature plasmas, Diam. Relat. Mater. 13 (4–8) (2004) 1177–1181.
[52] C. Stringer, T. Wang, M. Michaelos, M. Pachitariu, Cellpose: a generalist algorithm for cellular segmentation, Nat. Methods 18 (1) (2021) 100–106.